

# Backbending in $^{50}\text{Cr}$

G. Martínez-Pinedo<sup>1)</sup>, A. Poves<sup>1)</sup>, L.M. Robledo<sup>1)</sup>  
E. Caurier<sup>2)</sup>, F. Nowacki<sup>2)</sup>, J. Retamosa<sup>2)</sup> and A. P. Zuker<sup>1,2)</sup>

<sup>1)</sup> *Departamento de Física Teórica C-XI. Universidad Autónoma de Madrid E-28049 Madrid, Spain*

<sup>2)</sup> *Division de Physique Theorique. Centre de Recherches Nucleaires F-67037 Strasbourg Cedex-2, France*

The collective yrast band and the high spin states of the nucleus  $^{50}\text{Cr}$  are studied using the spherical shell model and the HFB method. The two descriptions lead to nearly the same values for the relevant observables. A first backbending is predicted at  $I = 10\hbar$  corresponding to a collective to non-collective transition. At  $I = 16\hbar$  a second backbending occurs, associated to a configuration change that can also be interpreted as an spherical to triaxial transition.

PACS number(s): 21.10.Re, 21.10.Ky

In a recent paper [1] we have shown that large scale Shell Model (SM) calculations with the realistic interaction KB3 predict the same intrinsic state than mean field calculations (Cranked Hartree-Fock-Bogoliubov) with the Gogny force for the ground state rotational band of  $^{48}\text{Cr}$ . Thus, we have two complementary views of the problem. For the SM wave functions have the proper quantum numbers (angular momentum and particle number) and include correlations in the wave functions needed for a detailed account of the observables, while the mean field results provide us with a simpler understanding of the intrinsic state on top of which the rotational ground state band is built. In this paper we proceed in the same way for the nucleus  $^{50}\text{Cr}$ . Experimentally [2], it is known that up to  $J = 10$  the Yrast states of  $^{50}\text{Cr}$  are members of a rotational band. The gamma ray energy of the last known state  $J = 12^+$  to the  $J = 10^+$  indicate that  $^{50}\text{Cr}$  has started to backbend at  $J = 10$  this situation being reminiscent of that encountered in  $^{48}\text{Cr}$ . The two additional neutrons of the nucleus  $^{50}\text{Cr}$  will contribute to the appearance of new structures when the angular momentum of the system is increased. As in the case of the Yrast band of  $^{48}\text{Cr}$ , where the backbending was due to a deformed to spherical transition, we find in  $^{50}\text{Cr}$  that the incipient backbending observed at  $J = 10$  is also due to a shape transition from the prolate  $J = 10$  state to the nearly spherical (actually slightly oblate)  $J = 12$  state. Contrary to what happens in  $^{48}\text{Cr}$  the Yrast band of  $^{50}\text{Cr}$  undergoes a second transition at  $J = 16$  from the slightly oblate regime to a more deformed, triaxial regime that causes a second backbend. The behaviour of the Yrast band of  $^{50}\text{Cr}$  can also be understood in terms of the changes of the occupancies of the  $1f_{7/2}$  orbitals of protons and neutrons.

**Computational procedures.** We shall briefly describe the computational procedures used in this paper. A more detailed account can be found in [1]. In the Spherical Shell Model (SM)  $^{50}\text{Cr}$  is described in a  $0\hbar\omega$  space, i.e. ten particles are allowed to occupy all the states available in the  $pf$  shell ( $\sim 10^7$ ). The effec-

tive interaction is the same used in the  $^{48}\text{Cr}$  calculation i.e., a minimally modified version of the Kuo-Brown's G-matrix [3] denoted KB3 in [4]. The single particle energies are taken from the  $^{41}\text{Ca}$  experimental spectrum. The effect of core polarization on the quadrupole properties is taken into account by the use of effective charges  $q_\pi = 1.5$ ,  $q_\nu = 0.5$ . These reasonable values agree with the estimation of core effects in the quadrupole properties carried out for  $^{48}\text{Cr}$  [1]. The secular problem is solved using the code ANTOINE [5], a very fast and efficient implementation of the Lanczos method.

In the intrinsic frame calculations we have used the Self Consistent Cranking Hartree-Fock-Bogoliubov method (HFB) with the density dependent Gogny force [6]. The mean field intrinsic states  $|\phi_\omega\rangle$  have been expanded in a triaxial harmonic oscillator basis  $|n_x n_y n_z\rangle$  with different oscillator lengths. Ten oscillator shells are included in this calculation in order to ensure the convergence of the mean field results. In our calculation we use the DS1 parameters set of the Gogny force [7]. Without further changes, this force has proven capable of describing successfully many phenomena, and in particular high spin behaviour [8].

**The Yrast band.** In fig. 1 the SM, HFB and experimental gamma ray energies  $E_\gamma(J) = E(J) - E(J-2)$  are plotted as a function of the angular momentum  $J$  for the Yrast band. The SM results are very close to the experimental data. The CHFB results follow the trend of the SM ones but are shifted downwards in energy indicating a much bigger static moment of inertia than in the SM and the experiment. In [1] it was argued that this behaviour is the result of a deficient treatment of pairing correlations by the HFB method in the weak pairing regime. However, this deficiency does not affect to the nature of the intrinsic state in a substantial way. The experimental results from the Chalk-River Mc Master collaboration [9], show preliminary evidence for Yrast states ( $14^+$  and  $16^+$ ) at excitation energies 9.9 MeV and 13.9 MeV. These results would confirm the existence of a first backbending in  $^{50}\text{Cr}$ . Notice that the corresponding  $E_\gamma$ 's, 2.3 MeV

and 4.0 MeV fit reasonably well into our predictions.

In both theoretical calculations a second backbending is predicted to take place at  $J = 16\hbar$ . Its origin will be discussed below in terms of the changes observed in the quadrupole moment and of the evolution of the occupancies of the relevant spherical orbits.

The quadrupole properties obtained in both approaches are summarized in Fig. 2. In the upper panel the  $\beta$  and  $\gamma$  deformation parameters obtained in the HFB calculation are plotted versus the angular momentum. We can interpret these results as defining three regions:

- At low angular momentum  $^{50}\text{Cr}$  is an axially symmetric prolate nucleus ( $\beta \sim 0.23$  and  $\gamma \sim 0$ )
- At  $J = 10\hbar$  the  $\beta$  value drops to 0.15 but the system is still axially symmetric while at  $J = 12\hbar$  the system undergoes a shape transition to a weakly deformed oblate state with  $\beta = 0.08$  and  $\gamma = -67$  degrees. This sudden change is responsible for the observed backbending at  $J = 10\hbar$ .
- At  $J = 16\hbar$  a new transition occurs that makes the system triaxial increasing at the same time the  $\beta$  value. These changes of the quadrupole moment are responsible for the backbending seen at  $J = 16\hbar$ .

In the middle panel the spectroscopic quadrupole moment of the SM calculation is plotted as a function of  $J$ .  $Q_s$  changes sign, from negative to positive at  $J = 10$ . This point has been recently discussed by Zamick and coworkers [10]. They made truncated shell model calculations using also the interaction KB3. Their results for the quadrupole moments at truncation level  $t=3$  are qualitatively equivalent to our full space results. Nevertheless, they interpret these positive quadrupole moments as pertaining to a “high K prolate” band [11] while we rather rely in the HFB results to conclude that these states are of oblate, non-collective character. This transition is correlated with the backbending in the  $E_\gamma$  plot. The spectroscopic quadrupole moment and the intrinsic deformations  $\beta$  and  $\gamma$  behave in a very similar way. However, it is difficult to establish a close connection between them in the high spin region where the  $K$  labeling is probably meaningless. In ref. [10] it was pointed out that the very large and negative values of  $Q_s$  for the states of highest spins correspond to those for the maximally aligned configurations. Our results agree with this interpretation. Triaxiality comes in because two or more of these configurations are simultaneously present in the wave function of these yrast states.

In the lower panel of Fig. 2 the  $B(E2)$  transition probabilities from the SM and HFB calculations are plotted as a function of  $J$  and compared with the available experimental data. The HFB results are obtained from the intrinsic values of the quadrupole operators  $Q_{20}$  and  $Q_{22}$

using an improved rotational formula [12]. Both results are very similar in the whole range of angular momentum considered. The comparison with the experiment data is good for the  $B(E2, 2^+ \rightarrow 0^+)$  but both theoretical results overestimate the experimental ones at  $J = 4$  and  $6\hbar$ .

In order to understand the behaviour of the previously considered observables as a function of  $J$  it is convenient to analyze the structure of the intrinsic states in terms of the “fractional shell occupancies”  $\nu(n, l)$  and the “shell contribution to  $\langle J_x \rangle$ ”  $j_x(n, l)$  defined in ref. [1]. In Figure 3 we have plotted the fractional occupancies of the spherical orbits in the HFB solution (upper panel) and in the SM one (middle panel). In addition the shell contributions to  $\langle J_x \rangle$  (which only make sense in the HFB calculation) are plotted for the relevant spherical orbits in the lower panel. There are striking similarities between the SM and HFB occupancies, with the HFB results being slightly smoother than the SM ones. Let us examine these numbers for the three regions sketched before.

Up to  $J = 8\hbar$  only the  $1f_{7/2}$  orbit and its  $\Delta j = 2$  deformation partner  $2p_{3/2}$  are appreciably occupied. This is in agreement with the fact that up to that value of the angular momentum the nucleus is an axially symmetric prolate rotor ( $\beta \sim 0.23$ ) as surmised in ref. [13]. The situation is the same than in  $^{48}\text{Cr}$ . For  $J = 8\hbar$  the occupation of the  $2p_{3/2}$  orbit starts decreasing in favor of the  $1f_{7/2}$ , as the later is more capable to create angular momentum. As a consequence the  $\beta$  deformation gets reduced (see Fig. 2) and the first backbending sets in.

At  $J = 12\hbar$  the  $2p_{3/2}$  orbit is emptied both for protons and neutrons eliminating the quadrupole coherence. In the lower panel we can see that the contribution of the neutrons to the total angular momentum,  $J = 12\hbar$ , is  $J = 6\hbar$  and comes fully from the  $1f_{7/2}$  orbit. But, six units of angular momentum is the maximum attainable by six identical particles in the  $1f_{7/2}$  orbit, therefore neutrons are fully aligned. In order to build up fourteen units of angular momentum the system chooses to align the four protons in the  $1f_{7/2}$  orbit to obtain  $J = 8\hbar$  (the other alternative is to move neutrons to higher orbits).  $J = 14\hbar$  is the maximum angular momentum that can be obtained with four protons and six neutrons in the  $1f_{7/2}$  orbit. Therefore, to reach  $J = 16\hbar$ , the system is forced to pump out particles of the low  $K$  states of the  $1f_{7/2}$  orbit to high  $K$  states of the  $1f_{5/2}$  as seen in the neutron occupancies plot. This leads to the second backbending because the excitation energy of the  $16^+$  state is anomalously large. When the  $1f_{5/2}$  neutron shell is exhausted (at  $J = 18\hbar$ ) the  $2p_{3/2}$  neutron shell enters into the game again. Placing particles in the  $2p_{3/2}$  increases again the quadrupole coherence producing the increase of deformation observed in Fig. 2. At  $J = 22\hbar$  the band terminates as the maximum angular momentum that can be built with four protons and six neutrons in the  $fp$  shell is  $23\hbar$ .

In figure 4 we present our predictions for the gyromagnetic factors compared with the experimental results of

Pakou *et al.* [14]. Once again the SM and HFB results are nearly identical for the whole band but they do not agree with the data except for the state  $J = 2$ . The situation is somehow puzzling. We know that  $^{50}\text{Cr}$  is not as good a rotor as  $^{48}\text{Cr}$ ; its  $B(E2)$ 's are smaller and the collectivity, as a function of the rotational frequency, vanishes earlier. Our descriptions of  $^{50}\text{Cr}$  tend to overshoot the experimental  $B(E2)$  values, indicating that possibly we are obtaining a too large quadrupole collectivity. However, for the gyromagnetic factors, the contrary seems to happen. We need to increase the quadrupole correlations in order to approach the rotational limit indicated by the experiment. It is difficult to move simultaneously in both directions. We have tried another version of the KB interaction called KB' in [15] that has a smaller gap between the  $2p_{3/2}$  and the  $1f_{7/2}$  orbits, thus favoring deformation. As we feared, while the  $g$  values get reduced ( $g(2^+) = 0.53$ ,  $g(4^+) = 0.60$ ,  $g(6^+) = 0.62$ ,  $g(8^+) = 0.66$ ) and nearly agree with the experimental results of ref. [14], the  $B(E2)$ 's increase a lot. For instance the  $4^+ \rightarrow 2^+$  transition has  $B(E2) = 415 \text{ e}^2\text{fm}^4$ , compared to the experimental value  $159(21) \text{ e}^2\text{fm}^4$  or to the KB3 value  $264 \text{ e}^2\text{fm}^4$ . Therefore we think that it will be extremely difficult to reproduce simultaneously the experimental  $g$  factors and the experimental  $B(E2)$ 's.

**Further discussion of the high spin region.** We have already shown that the double backbending in  $^{50}\text{Cr}$  is related to the existence of three different zones in the yrast line, and takes place in the two interphases. In the first of those regions, up to  $J = 10\hbar$  the decay proceeds by the usual sequence of  $\Delta J = 2$  enhanced E2 transitions. Here we shall study the decay patterns in the other two zones.

In figure 5 we have plotted the yrast band as given by the SM calculation, from the first backbending to the maximum  $J$  attainable in the  $(1f_{7/2})^{10}$  configuration. A new feature is evident: beyond  $J = 10\hbar$  the yrast sequence shows up as  $\Delta J = 1$ . Therefore, the decay may become more complex, in particular M1 transitions are now allowed. And not only allowed but dominant due to the hampering of the quadrupole collectivity in this zone. In the figure we can follow the decay subsequent to the feeding of the  $J = 14\hbar$  state. Indeed the emitted gammas are mostly M1, only the  $14^+ \rightarrow 12^+$  is dominantly E2. The figure also presents our predictions for the lifetimes and branching ratios using the measured  $E_\gamma$ 's. Experimental results from the Mc Master Chalk River collaboration and from Legnaro [16] are expected to come out soon.

It is quite exciting to find out that the yrast decay at the first backbending proceeds via magnetic transitions.

Let's now move higher in energy and angular momentum. If we assume that the yrast band is fed at the yrast  $18^+$  state, the dominant decay sequence will be:

$$18_1^+ \xrightarrow{E2} 16_1^+ \xrightarrow{E2} 14_2^+ \xrightarrow{E2} 12_1^+$$

If we choose the yrast  $17^+$  state as entry point; the decay sequence will be:

$$17_1^+ \xrightarrow{E2} 15_1^+ \xrightarrow{E2} 13_2^+ \xrightarrow{M1} 12_1^+$$

Hence, in the third zone we recover the  $\Delta J = 2$ , E2 decay pattern, in spite of the fact that the yrast sequence is now  $14^+ - 15^+ - 16^+ - 17^+ - 18^+$ . The surprising thing is that the decay bypasses the yrast  $14^+$  and  $13^+$  states, a striking feature associated to the second backbending.

In conclusion, we have shown that the spherical shell model and the Cranked Hartree Fock Bogolyubov method give similar -and accurate- descriptions of  $^{50}\text{Cr}$ . In particular, they predict two backbendings in the  $E_\gamma$  plot of the yrast band, which are interpreted as due to two changes of regime: first from collective prolate to non-collective oblate and second from  $(1f_{7/2})^{10}$ -dominated configurations to aligned states with less than ten particles in the  $1f_{7/2}$  shell. A puzzling situation is found in the collective, low energy part of the yrast band, where the calculations fail to reproduce the experimental gyromagnetic factors. Finally in our study of the decay sequence from the high spin yrast states we have found out that the decay mode varies from one zone to another. In the high spin regime it proceeds by stretched E2 transitions, at the first backbending by M1's and in the lower part by collective E2's. At the second backbending the decay sequence bypasses the yrast line .

We thank Dr. J. A. Cameron for making his results available to us before publication. This work has been partially supported by the DGICYT, Spain under grants PB93-263 and PB91-0006, and by the IN2P3-(France) CICYT (Spain) agreements. A. Z. is Iberdrola Visiting Professor at the Universidad Aut3noma de Madrid.

- 
- [1] E. Caurier, J.L. Egido, G. Mart3nuez-Pinedo, A. Poves, J. Retamosa, L.M. Robledo and A. Zuker, Phys. Rev. Lett. **75**, 2466 (1995)
  - [2] T.W. Burrows, Nuclear Data Sheets (1990)
  - [3] T.T.S. Kuo and G.E. Brown, Nucl. Phys. **A114**, 241 (1968)
  - [4] A. Poves and A. Zuker. Phys. Rep. **70**, 235 (1981)
  - [5] E. Caurier, code ANTOINE, Strasbourg 1989.
  - [6] D. Gogny. *Nuclear Selfconsistent fields*. Eds. G. Ripka and M. Porneuf (North Holland 1975).
  - [7] J.F. Berger, M. Girod and D. Gogny. Nucl. Phys. **A428**, 23c (1984).
  - [8] J.L. Egido, L.M. Robledo, Phys. Rev. Lett. **70**, 2876 (1993); J.L. Egido, L.M. Robledo and R.R. Chasman,

- Phys. Lett. **322B**, 22 (1994); M. Girod, J.P. Delaroche, J.F. Berger and J. Libert, Phys. Lett. **325B**, 1 (1994).
- [9] J. A. Cameron, private communication.
- [10] L. Zamick, M. Fayache and D.C. Zheng. Phys. Rev. C **53** 188 (1996).
- [11] L. Zamick and D.C. Zheng, LANL archive nucl-th/9603012.
- [12] J. L. Egido and H. Weidenmuller, Phys. Rev. C **39**, 2398 (1989).
- [13] A. Zuker, J. Retamosa, A. Poves and E. Caurier, Phys. Rev. **C52**, R1742 (1995).
- [14] A.A. Pakou, J. Billowes, A.W. Mounford and D.D. Werner. Phys. Rev. C **50**, 2608 (1994).
- [15] E. Caurier, A.P. Zuker, A. Poves and G. Martínez-Pinedo, Phys. Rev. C **50**, 225 (1994).
- [16] S. Lenzi, private communication.

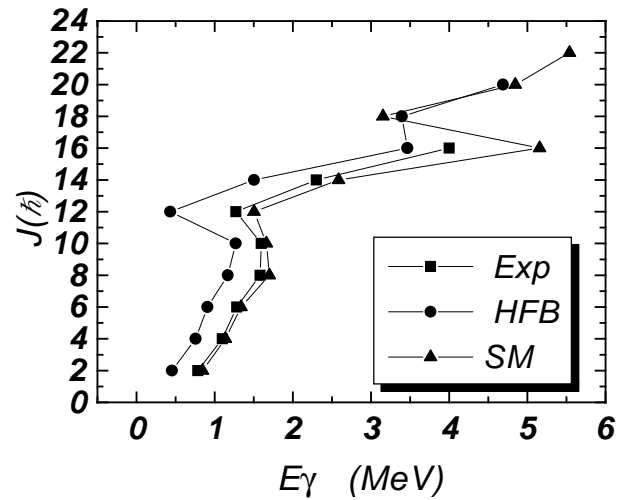


FIG. 1. Theoretical (triangles, SM; circles HFB) and experimental (squares) gamma ray energies versus the angular momentum  $J$

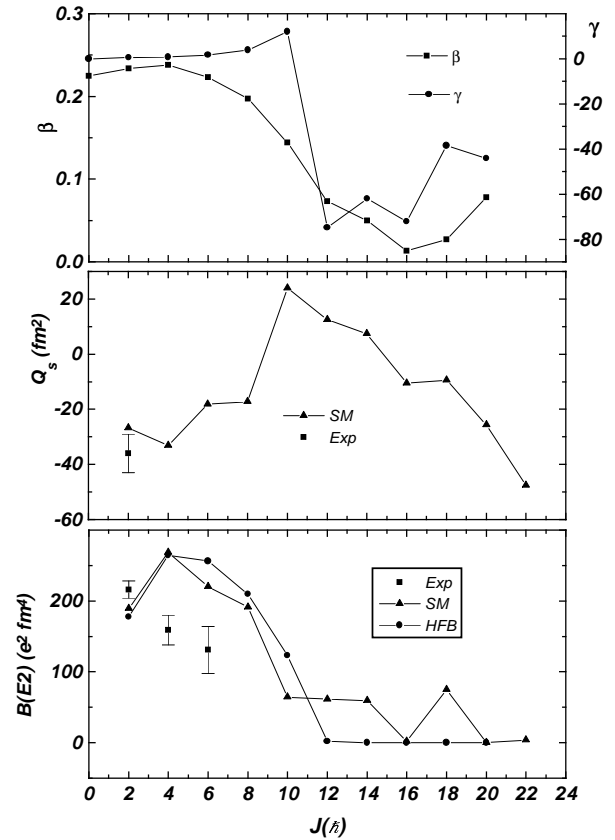


FIG. 2. Upper panel:  $\beta$  and  $\gamma$  deformations in the HFB calculation. Middel panel: Spectroscopic quadrupole moment  $Q_s$  computed in the SM approach. The experimental value  $Q_s(2^+)$  is also given. Lower panel:  $B(E2, J \rightarrow J-2)$  transition probabilities versus  $J$  computed in SM (triangles) and HFB (circles) compared to the experimental data (squares)

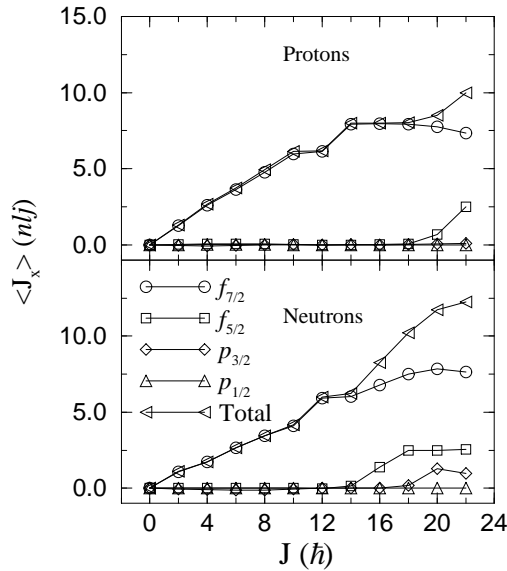
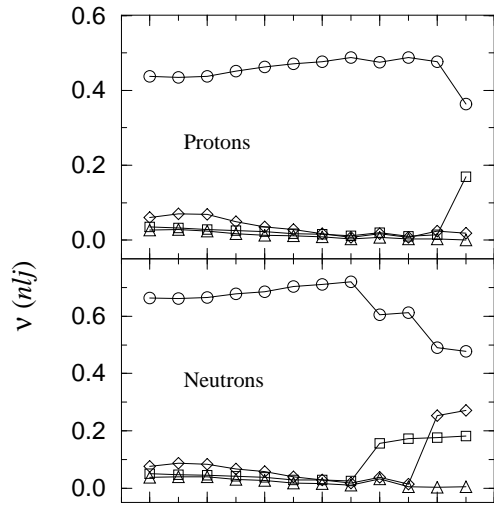
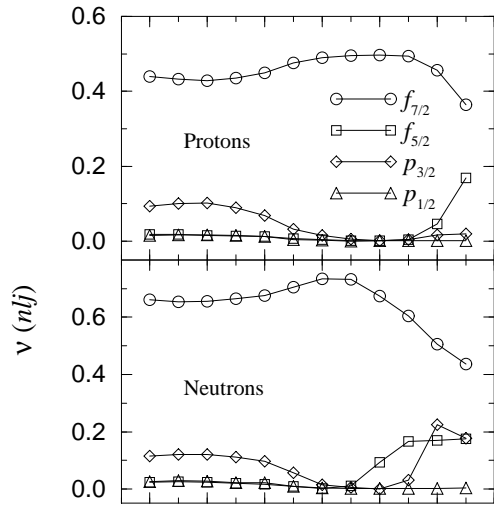


FIG. 3. Upper panel: “Fractional shell occupancies”  $\nu(n, l)$  computed in the HFB approach as a function of  $J$ . Middle panel: Same as before but for the SM. Lower panel: “Shell contribution to  $\langle J_x \rangle$ ”  $j_x(n, l)$  in HFB.

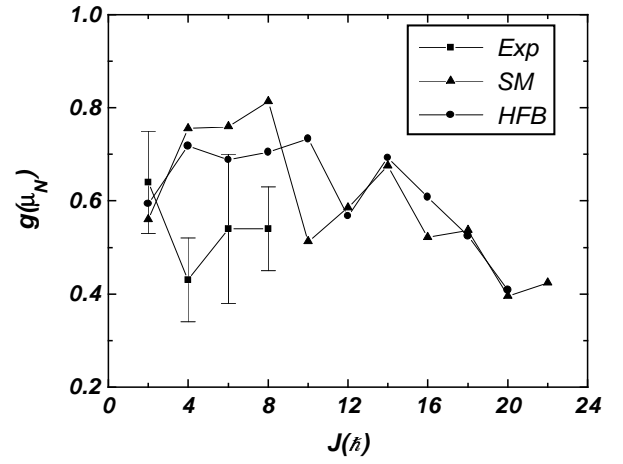


FIG. 4. Gyromagnetic factors: SM (triangles), HFB (circles) and experiment (squares).

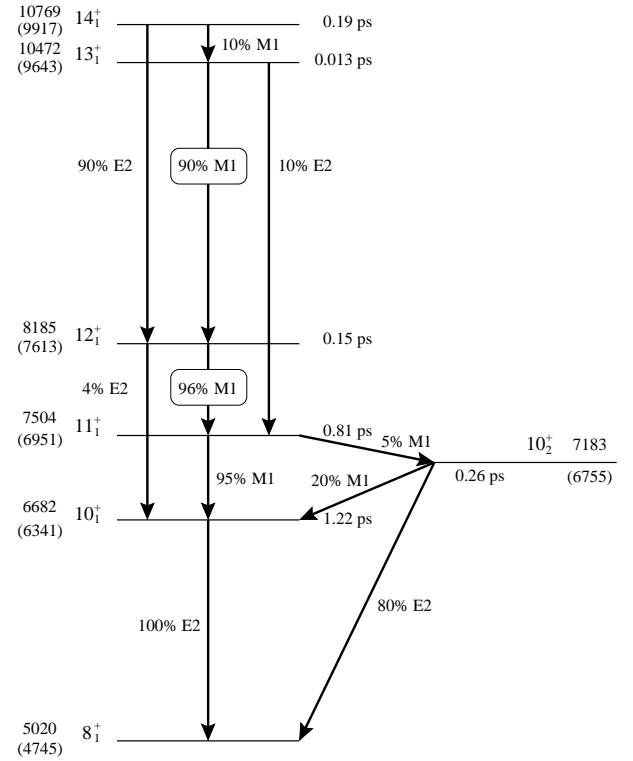


FIG. 5. Decay scheme in the region of the first backbending. Energies in keV. In parenthesis the experimental values.